Sodium-induced embrittlement of an aluminum grain boundary

Shengjun Zhang,[1,*] Oleg Y. Kontsevoi,[2] Arthur J. Freeman,[1,2] and Gregory B. Olson[1]

[1]*Department of Materials Science and Engineering, Northwestern University, Evanston, Illinois 60208, USA*
[2]*Department of Physics and Astronomy, Northwestern University, Evanston, Illinois 60208, USA*

Primary aluminum produced industrially by electrolysis inevitably contains some sodium which is an undesired impurity element in aluminum alloys as it promotes intergranular fracture. However, the physical origins of Na-induced intergranular embrittlement in aluminum are still unclear. This work provides a comprehensive investigation of the nature of the Na-induced grain-boundary embrittlement in aluminum by means of first-principles calculations with the highly precise full-potential linearized augmented plane-wave method within the framework of the Rice-Wang thermodynamic model and within the method of *ab initio* tensile test. We introduce a free-surface slab model and determine the grain-boundary and free-surface energies, the most energetically favorable segregation site of Na along the Al grain boundary, its segregation energy to the Al grain boundary, and the possible fracture modes of the grain boundary with Na in the different sites and their corresponding fracture energies. We establish that Na has a large driving force (-0.84 eV/atom) to segregate from Al bulk to the symmetrical grain-boundary core site, and its segregation significantly reduces grain-boundary strength. We show that the method using the Rice-Wang thermodynamic model and the method of *ab initio* tensile test are essentially equivalent and both confirmed that Na is a strong intergranular embrittler with a potency of $+0.62$ eV/atom. Na segregation leads to grain-boundary expansion and a significant charge density decrease over the whole grain boundary. Analysis in terms of the relaxed atomic and electronic structures and bonding characters shows that the aluminum-sodium bond has ionic character and is weak in both grain-boundary and free-surface environments.

I. INTRODUCTION

It is now well recognized that mechanical properties, such as the brittleness of an engineered material, can be significantly changed by a small quantity of impurities segregating to grain boundaries (GBs).[1] Sodium is an undesired impurity element in aluminum alloys and its solubility in face-centered-cubic (fcc) Al is very low.[2] Primary Al is produced by the Hall-Héroult process, through the electrolysis of the mixture of molten alumina and cryolite ($Al_2O_3 + Na_3AlF_6$), the latter being added to lower the melting point.[3] Therefore Al, without further treatment, inevitably contains some Na ($>0.002\%$) and the content of Na in Al is influenced by the thermodynamics and kinetics of the electrolysis.

Various tensile test studies have shown that trace amounts of Na can drastically reduce the ultimate tensile strength and reduction of area of aluminum.[4] Although Na is not detected successfully on the fracture surface via Auger electron spectroscopy (AES),[4] it is widely believed that Na-induced high-temperature embrittlement in Al is associated with Na segregation to Al GBs which promotes GB embrittlement (GBE). A fundamental thermodynamic investigation[5] and some first-principles investigations[6,7] of Na-induced GBE in Al have been done but the nature of the phenomenon still needs further clarification. The aim of this research is to gain a comprehensive understanding of the mechanism of the Na-induced GBE through state-of-the-art first-principles investigations.

There are two most used *ab initio* approaches to investigate impurity-induced GBE theoretically: (i) one prevalent approach is based on a thermodynamic theory developed by Rice and Wang[8] which treats the competition between plastic crack blunting and brittle boundary separation. The potency of a segregation impurity in reducing the "Griffith work[9]" of brittle boundary separation is a linear function of the difference in binding energies for that impurity at the GB and at the free surface (FS). That is, if the GB is more energetically favored by an impurity than the FS, its resistance to brittle intergranular fracture is enhanced by this impurity. If the GB is less energetically favored by an impurity than the FS, its resistance to brittle intergranular fracture is weakened by this impurity. This method describes the effect of an impurity on intergranular embrittlement from an energy point of view and has been successfully applied previously to Fe and Ni GBs.[10–14]

(ii) Another method is the so-called *ab initio* tensile test or cleavage test. A uniaxial tensile strain is applied in the direction normal to the GB plane via extension of the supercell by a small increment, and then all atoms are allowed to fully relax. The computed total energy and separation distance is used to calculate both the total separation energy equivalent to Rice-Wang and the theoretical tensile strength of the GB. This method has been successfully applied previously to Ni and Al GBs.[15,16]

In this work, a comprehensive study is performed to investigate the Na-induced GBE in aluminum via first-principles calculations using both the Rice-Wang model and the *ab initio* computational tensile test. The highly precise full-potential linearized augmented plane-wave (FLAPW) method[17] is employed. At first, the GB and new FS models are introduced. The optimum size of the GB model is determined to minimize artificial size effects. A new FS model is presented to eliminate the interaction between the impurity atoms on two opposite surface of a FS slab. After calculating the pure Al GB and clean Al FS energies, the segregation
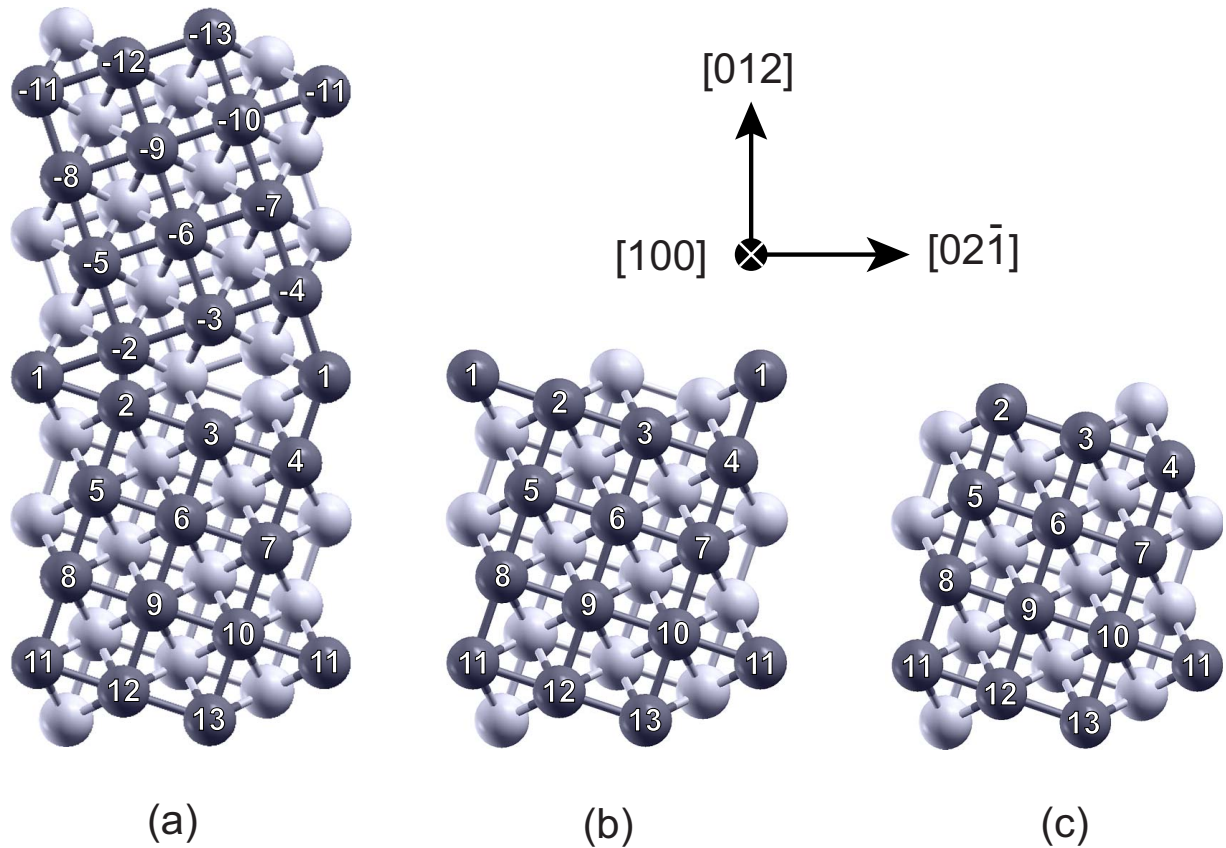
FIG. 1. (Color online) Crystal structures of (a) an Al $\Sigma5(012)[100]$ GB and two Al (012) FSs; (b) a 13-layer FS with Al core atom; and (c) a 12-layer FS without Al core atom. The atomic sites are labeled by numbers counted from the GB plane. The structures repeat along $[02\bar{1}]$ direction. The dark gray and light gray atoms represent atoms in layers with $y=0$ (in the paper plane) and $y=0.5$ (beneath the paper plane) along the $[100]$ direction, respectively. Site 1 is on the mirror plane; sites i and $-i$ ($i=2-13$) have mirror symmetry. The three directions $[100]$, $[012]$, and $[02\bar{1}]$ are shown by arrows. The $[012]$ direction is parallel to the z axis, whose length is optimized for the GB case.

energy of Na from Al bulk to the Al GB is calculated to validate the driving force of Na segregation. Then, the most energetically favored site of Na along the Al GB is determined. Following that, fully relaxed atomic structures of the GB and FS with and without Na are obtained by minimizing the total energies as directed by the calculated atomic forces. The calculated atomic and electronic features and theoretical tensile stress data are then used to analyze the physics which dominates the embrittling or strengthening behavior of Na in the Al GB.

II. GRAIN-BOUNDARY AND FREE-SURFACE MODELS

In this work, the symmetrical tilt Al $\Sigma5(012)[100]$ GB was chosen since it is a high energy and stable GB in Al according to experiments.[18] According to the profile of the measured relative energies of $[100]$ tilt GBs in Al as a function of misorientation angle,[18] an Al $\Sigma5(012)[100]$ GB has almost the highest GB energy. Since high-energy GBs tend to break before low-energy GBs, an Al $\Sigma5(012)[100]$ symmetrical tilt GB is a good candidate to study the GBE in Al.

The $\Sigma5(012)[100]$ notation refers to a special orientation between fcc crystals for which one in five lattice points are

coincident, and $[100]$ and (012) denote the crystal Miller indices of the axis of the misorientation and the habit plane of the GB, respectively. The initial positions of atoms in this GB were obtained using the coincident site lattice (CSL) model.[19]

Figure 1 represents the crystal structures of GB and FS based on the CSL model. Both GB and FS with and without a Na atom were simulated by a single slab model, which can minimize the interactions between GB images otherwise inherent in the traditional three-dimensional superlattice cell. There is only a two-dimensional (2D) translational symmetry in the slab model, which means that the cell does not repeat periodically along the z axis ($[012]$ direction).

For the GB system, a 25-layer slab model was adopted to simulate the clean Al $\Sigma5(012)[100]$ GB, which proved to be sufficiently large using a series of total-energy convergence tests discussed later. The GB system is composed of two identical grains, each containing 13 layers with one layer on the GB plane being shared between the two grains. A vacuum region with a 4.5 a.u. thickness is added on both sides. The atom belonging to the shared plane, which we will call a "core atom," is marked as site 1 in Fig. 1. There is a mirror symmetry in the clean GB, so the sites $-i$ and i ($i=2-13$) are equivalent. One Na atom is placed near the GB

core in each unit cell replacing an Al atom. The energetic preference site (1, 2, or 3) of a Na atom along GB was then determined.

In the previous works,[10–14] the FS model with two impurities on the opposite surfaces of the model in each unit cell was employed. In such a model there could be an artificial interaction between the impurities on the opposite sides due to the limited FS cell size. Also, the previous FS model was not closely related to the GB structure. In this work, a new FS slab model is introduced which is directly associated with the GB model: as shown in Figs. 1(b) and 1(c), the two new FS structures represent the GB model after it breaks. Only one impurity atom was put in one side of the FS slab, and the other side (sites 11–13) is treated as a bulklike structure. Thus, in contrast to the previous FS models, there is no interaction between impurity atoms on opposite sides of the slab. Vacuum regions with 4.5 a.u. thickness are added above both the fractured FS and the bulklike end side.

III. COMPUTATIONAL METHOD

The FLAPW method has proven to be one of the most accurate methods for the computation of the electronic structure of solids within density-functional theory. The FLAPW method for thin films[17] was employed, which utilizes a two-dimensional basis set and thus does not require creation of artificial supercells. No shape approximations are made to the charge densities, potentials, and matrix elements. For both the aluminum and Na atoms, the core states are treated fully relativistically and the valence states are treated semi-relativistically (i.e., without spin-orbit coupling). The exchange correlation contribution to the potential was included using the generalized gradient approximation (GGA) within the Perdew-Burke-Ernzerhof functional.[20] An energy cutoff of 218 eV was employed for the augmented plane-wave basis to describe the wave functions in the interstitial region, and a 1100 eV cutoff was used for the star functions depicting the charge density and potential. Muffin-tin radii for Al and Na atoms were both chosen as 2.3 a.u. and the 2D **k**-point mesh is 7×7. Within the muffin-tin spheres, lattice harmonics with angular momentum quantum number l up to 8 were adopted to expand the charge density, potential, and wave functions.

Convergence was assumed when the average root-mean-square differences between the input and output charge and spin densities are less than 1×10^{-5} $e/(a.u.)^3$. The equilibrium atomic positions in both the in-plane and the out-of-plane directions of both the Na/Al FS and Na/Al GB systems, and their corresponding clean reference systems, were determined according to the calculated atomic forces. In order to simulate the bulklike environment for the GB case, we fixed the positions of the three outermost Al layers (sites 11, 12, 13, and −11, −12, −13) to their fcc coordination and distances in bulk Al; all other atoms in the unit cell were fully relaxed by force minimization using a damped Newton scheme. Equilibrium relaxed structures were assumed when the atomic forces on each atom became less than 0.01 eV/a.u. Likewise, three outermost Al layers at one end side of the FS model were fixed to simulate the bulklike environ-

ment and other layers were allowed to relax. This makes the second side of the FS slab to be exactly like the surface of the GB slab. As will be shown in the following sections, in all equations to calculate the embrittling potency and other quantities of interest only the differences between total energies of GB and FS enter, therefore the total-energy contributions from the fixed GB and FS surfaces will cancel out, and the FS model will effectively have only one surface. Thus, the way how the GB and FS models are built and relaxed in this work results in the removal of errors arising from surface effects and makes the calculated physical and mechanical properties more accurate and reliable.

IV. GB AND FS MODELS BUILDING AND VALIDATION

A. Lattice constant of Al in the fcc structure

The precise lattice constant of an Al in the fcc structure was determined at first by a series of calculations using different **k**-point meshes and cut-off energies. An optimum **k**-point mesh $(15 \times 15 \times 15)$ and cut-off energy (275 eV) were determined. The calculated lattice constant is 4.039 Å at 0 K compared with experimental 4.0495 Å at 296 K.[21] This theoretical lattice constant is used later in the slab model of the Al GB. The calculated bulk modulus is 77.5 GPa at 0 K compared with experimental 76 GPa at 298 K.[22] The calculated results are in good agreement with the experimental data.

B. Optimization of the GB and FS models

An ideal CSL model of the GB with atoms at lattice points was used as an initial configuration. However, the mathematical CSL model does not take into account atomic size, and a strain might exist in the GB system. For example, sites 2 and −2 in the CSL model of $\Sigma 5(012)[100]$ GB are close to each other, and the model should be relaxed to release the strain between the two grains. This was done by expanding the GB model in the direction of the z axis in small increments and calculating the total energy of each configuration. The minimum of the curve of the total energy of the GB system versus the expansion corresponds to the equilibrium GB.

Further, an optimum number of layers of the GB model should be chosen. The increase in the number of layers will reduce artificial interactions between GB and the surfaces of the GB slab model; however, the computational requirements will also increase. To find a balance, a series of clean GBs with different number of layers (i) were calculated. The number of layers was consequentially increased by two (to preserve the symmetry), and the energy of each added layer E^i was calculated as

$$2E^i = E(i+2) - E(i), \qquad (1)$$

where $E(i+2)$ is the total energy of a clean GB with $(i+2)$ layers and $E(i)$ is the total energy of a clean GB with i layers. The size effect is then calculated as $\Delta E^i_{size} = E^i - E^{i+2}$. The optimum number of layers in the GB model can be determined when ΔE^i_{size} becomes sufficiently small. After calculating a series of GB models with the number of layers from

11 to 31, it was determined that the optimal number of layers in the Al GB model is 25 since ΔE_{size}^{i} becomes sufficiently small (0.01 eV) when adding two more layers. This corresponds to FS models with 12 and 13 layers. The equilibrium expansion of this 25-layer pure Al GB system is 0.45 a.u. with respect to the initial CSL configuration.

C. Structure and energy of Al Σ5(012)[100] GB and (012) Al FS

The GB and FS energy is defined as the total-energy difference between GB/FS system and fcc Al bulk. The pure Al GB energy is calculated as follows:

$$\Delta E(\text{GB}) = \frac{E_{\text{GB}}^{25\text{-layer}} - E_{Bulk}^{25\text{-layer}}}{S}, \qquad (2)$$

Where $E_{\text{GB}}^{25\text{-layer}}$ is the total energy of a 25-layer Al Σ5(012)[100] symmetrical tilt GB, $E_{Bulk}^{25\text{-layer}}$ is the total energy of a 25-layer Al slab oriented along the (012) plane without the GB which represents Al bulk, and S is the unit cell area of the (012) plane thereafter. Our calculated GB energy is 0.501 J/m^2 at 0 K. This result is consistent with measurements of the average GB energy in pure Al of 0.324 J/m^2 at 723 K and 0.380 J/m^2 at 298 K by thin film transmission electron microscopy techniques[23] and also agrees with previous calculated results of 0.600 J/m^2 (Ref. 18) and of 0.411 J/m^2 (Ref. 24) at 0 K.

Since two pure Al (012) FS are generated after the Al bulk breaks, the pure Al (012) FS energy is calculated as follows:

$$\Delta E(\text{FS}) = \frac{E_{\text{FS}}^{13\text{-layer}} + E_{\text{FS}}^{12\text{-layer}} - E_{Bulk}^{25\text{-layer}}}{2S}, \qquad (3)$$

where $E_{Bulk}^{25\text{-layer}}$ is again the total energy of a 25-layer Al slab oriented along the (012) plane without the GB, $E_{\text{FS}}^{13\text{-layer}}$ is the total energy of a 13-layer Al (012) FS and $E_{\text{FS}}^{12\text{-layer}}$ is the total energy of a 12-layer Al (012) FS. Our calculated (012) FS energy is 1.016 J/m^2, which is slightly more than twice the energy of the Al Σ5(012)[100] GB. This result is in good agreement with measurements of the average FS energy in pure Al of 0.980 J/m^2 at 723 K and 1.150 J/m^2 at 298 K by thin film transmission electron microscopy techniques.[23] Commonly, the GB energy is approximately half the FS energy for metals and ceramics. Our results are consistent with this general trend.

The fracture energy of the Al GB is defined as the energy needed to break the Al GB into two fracture surfaces and can be calculated as

$$\Delta E(fracture) = \frac{E_{\text{FS}}^{13\text{-layer}} + E_{\text{FS}}^{12\text{-layer}} - E_{\text{GB}}^{25\text{-layer}}}{S}$$

$$= 2\Delta E(\text{FS}) - \Delta E(\text{GB}). \qquad (4)$$

The value of the calculated fracture energy is 1.531 J/m^2. The calculated GB energy and fracture energy of the Al Σ5(012)[100] symmetrical tilt GB and (012) Al FS energy in comparison with experimental data and previous calculated results are summarized in Table I.

The calculated interlayer distances for the clean Al GB are plotted in Fig. 2(a). An oscillatory displacement occurs in

TABLE I. Calculated GB energy and fracture energy of Al Σ5(012)[100] symmetrical tilt GB and (012) Al FS energy (J/m^2), in comparison with experimental data and previously calculated results.

Energy	Value (J/m^2)	Temperature (K)	Method	Reference
GB energy	0.501	0	Calculation	This work
	0.324	723	Experiment	23
	0.380	298	Experiment	23
	0.600	0	Calculation	18
	0.411	0	Calculation	24
FS energy	1.016	0	Calculation	This work
	0.980	723	Experiment	23
	1.150	298	Experiment	23
Fracture energy	1.531	0	Calculation	This work

the vicinity of the Al GB. The dashed line is the calculated bulk interlayer distance (1.707 a.u.). The largest interlayer distance is between layers 1 and 2 (or −2), which is larger
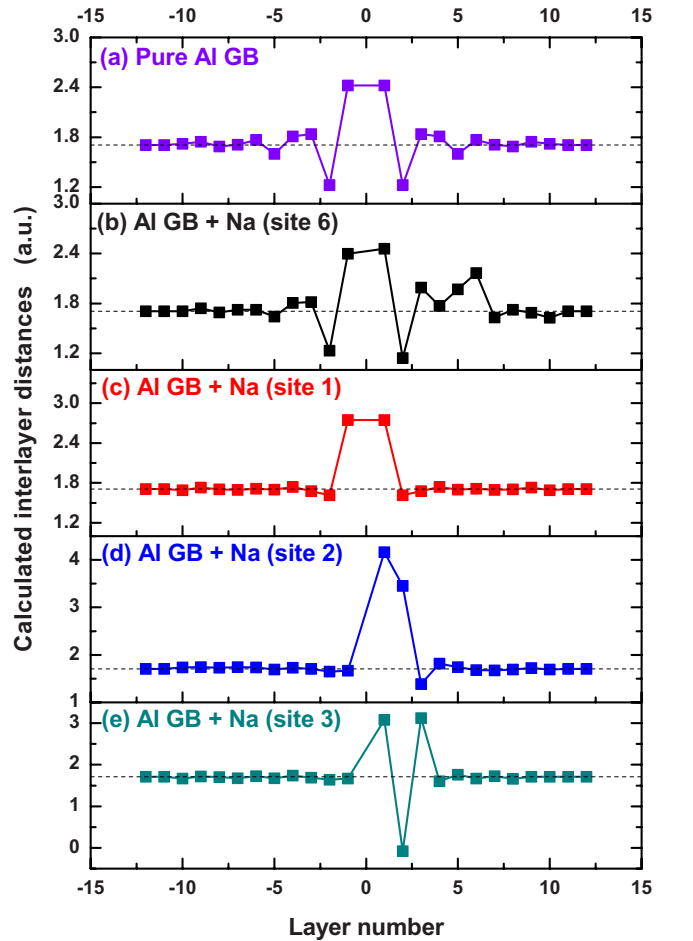
FIG. 2. (Color online) Calculated interlayer distances (a.u.) in GB systems with and without one Na atom vs the distance between the ith and jth layers. The calculated bulk interlayer distance is 1.707 a.u. which is shown by the dashed line as a reference. Note that the positions of layers 11, 12, 13, −11, −12, and −13 are fixed.
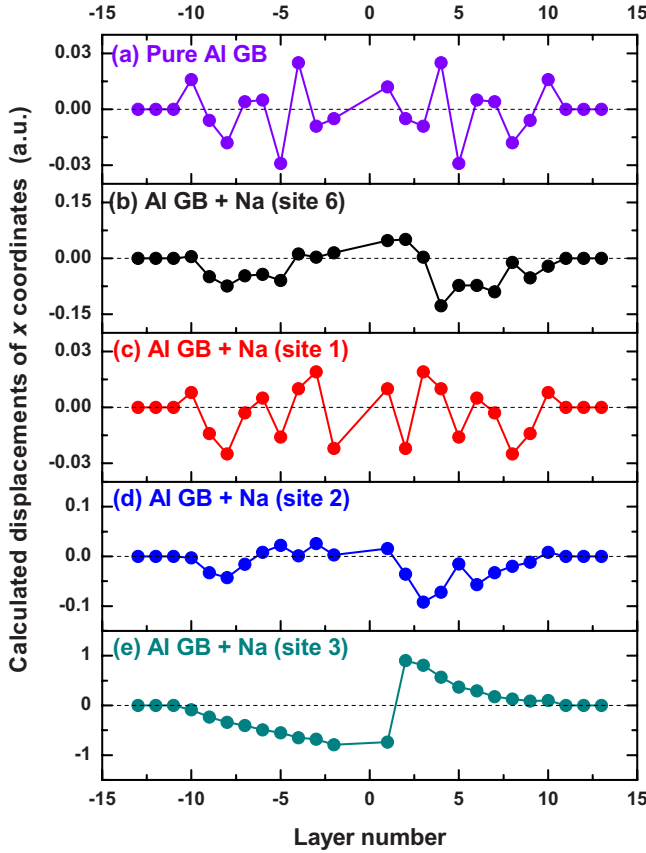
FIG. 3. (Color online) Calculated displacements of x coordinates (a.u.) relative to the ideal $\Sigma 5(012)[100]$ Al GB. Note that the coordinates of atoms in layers 11, 12, 13, -11, -12, and -13 are fixed.

than the distance in bulk Al by as much as 0.717 a.u. It is a result of a repulsion between interfacial Al(2) and Al(-2) layers across the GB. This expansion is partially compensated for by the reduced distance between layers 2 and 3, which is smaller than the interlayer distance in bulk Al by 0.483 a.u. Still, the Al(3) and Al(-3) layers are pushed away from the ideal positions obtained according to the CSL model by 0.235 a.u., layers Al(4) and Al(-4) by 0.365 a.u., and Al(5) and Al(-5) by 0.467 a.u. This expansion creates a larger "hole" in the GB which can act as a segregation site for interstitial impurities. Overall, there is a long-range oscillatory pattern for the Al interplanar distances away from the GB, as commonly observed in surfaces and interfaces.

In previous calculations of the GB,[10–14] only the relaxation normal to the GB plane was allowed, and the in-plane displacements were often assumed to be very small and were ignored for calculation efficiency. In this work, displacements in the (100) plane were fully taken into account. The calculated displacements of x coordinates are shown in Fig. 3(a), where it is found that some displacements are too large to be ignored. Relaxation of the atom positions along the x axis as well as the z axis allow us to obtain the lowest global total energy of the system. A similar oscillation of displacements occurs in the vicinity of the Al GB. The Al(1) moves along the x axis by 0.012 a.u. while Al(2) and Al(-2) move 0.005 a.u. in the opposite direction, and so on.
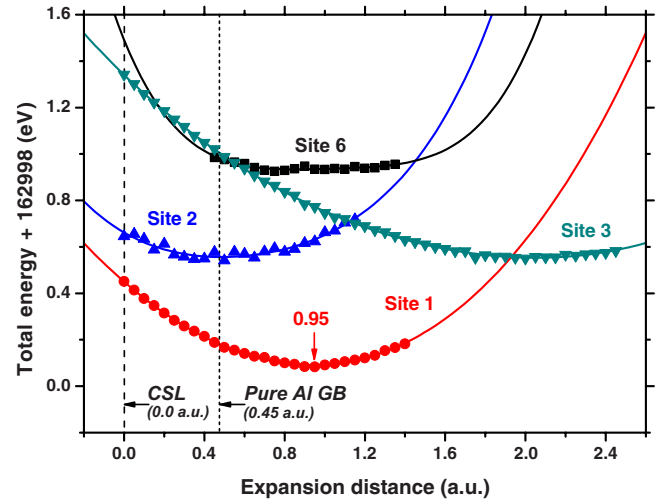
FIG. 4. (Color online) The total energy of the bulk Al and GB with a Na atom in different positions with respect to the expansion of the cell relative to CSL model size.

V. PREFERRED SEGREGATION SITE OF A Na ATOM IN THE GB

A. Segregation energy

Before investigating the effect of Na on the Al GB fracture energy, the segregation energy of Na was determined to show whether a Na atom will segregate energetically from Al bulk to the Al GB. The segregation energy is the energy needed for a Na atom to diffuse from a bulk site to a GB site and can be calculated using

$$\Delta E_{\text{Na}}^{Seg} = E_{\text{Na}}^{Bulk} - E_{\text{Na}}^{\text{GB}}, \tag{5}$$

where E_{Na}^{Bulk} is the total energy of the system with a GB and a Na atom in a bulk site, and $E_{\text{Na}}^{\text{GB}}$ is the total energy of the system with a GB and a Na atom in a site along the GB.

The site 6 was chosen as a bulklike site to put one Na atom when calculating E_{Na}^{Bulk} because sites 1–4 are along the GB; sites 11–13 are fixed in the calculation; site 5 is close to the GB; and sites 7–10 are close to the surface of the model. Since the atomic size of Na is larger than that of Al, a Na atom prefers to occupy a substitutional site along the GB rather than the GB interstitial site. In previous first-principles studies, the substitutional impurity atom was always put on the core site in the mirror plane (site 1) of the GB. In this work, three different substitutional sites (1–3) along the GB were considered to calculate $E_{\text{Na}}^{\text{GB}}$, and the most energetically favorable site was identified.

The total energy of the system versus the expansion distance was calculated to obtain the equilibrium state for each case and the curves are plotted in Fig. 4. The GB with a Na atom in site 1 has the lowest energy compared with the GB with a Na atom in site 2 and site 3. For the GB with a Na atom in site 6, the total-energy curve vs expansion distance is higher than the other three cases with a Na atom along the GB. The calculated sort order of energies is $E_{\text{Na}}^{\text{GB}(site\ 1)} < E_{\text{Na}}^{\text{GB}(site\ 3)} < E_{\text{Na}}^{\text{GB}(site\ 2)} < E_{\text{Na}}^{Bulk}$, where the energies are taken at the minimum of the corresponding curves. Site 1 is the most energetically favorable site but there is also a driving

TABLE II. Calculated segregation energies, binding energies, and embrittling potencies of a Na atom at different sites in the Al GB.

Position along GB	Expansion distance (a.u.)	Segregation energy (eV/atom)	Fracture mode			Fracture energy (J/m^2)	$\Delta E_{\text{GB}} - \Delta E_{\text{FS}}$ (eV/atom)	Effect
			Mode	Part I	Part II			
Site 1	0.95	−0.84	1	12-layer Al	13-layer including Na	0.987	0.62	Strong embrittler
Site 2	2.00	−0.37	2-1	12-layer Al	13-layer including Na	1.144	0.44	Strong embrittler
			2-2	13-layer Al	12-layer including Na	0.571	1.10	Strong embrittler
			2-3	11-layer Al	14-layer including Na	0.558	1.19	Strong embrittler
Site 3	0.50	−0.38	3-1	12-layer Al	13-layer including Na	1.802	−0.31	Cohesion enhancer
			3-2	13-layer Al	12-layer including Na	1.119	0.47	Strong embrittler
			3-3	14-layer Al	11-layer including Na	1.214	1.11	Strong embrittler
			3-4	10-layer Al	15-layer including Na	1.135	0.48	Strong embrittler

force for segregation to the other sites from the bulk.

The sort order of the equilibrium expansion distances relative to the CSL model is $D_{\text{Na}}^{\text{GB}(site\ 3)} < D_{\text{Na}}^{Bulk} < D_{\text{Na}}^{\text{GB}(site\ 1)} < D_{\text{Na}}^{\text{GB}(site\ 2)}$. Considering that site 2 is the most compressed site, site 3 is the loosest site along the GB, and the compressive environment around bulk site 6, these calculated results correlate with the size difference between Al and Na atoms.

Using the calculated segregation energies, the Na concentration in the GB can be estimated according to the McLean equation,[25]

$$\frac{C_{\text{GB}}}{1 - C_{\text{GB}}} = C_{Bulk} \exp\left(\frac{-E_{\text{Na}}^{\text{GB}(site\ 1)}}{RT}\right), \quad (6)$$

where C_{GB} and C_{bulk} are the Na concentrations in the GB and bulk, respectively, T is the absolute temperature, and R is the universal gas constant. From the calculated segregation energy of −0.84 eV/atom and assuming the Na concentration in the bulk Al to be 1 parts per million (ppm), we find that the equilibrium Na concentration in the GB is 0.95 at the typical embrittlement temperature of 673 K. This indicates that the GB will be filled with almost a monolayer of the segregated Na atoms. The diffusivity of Na in the Al bulk was experimentally determined by Ransley and Neufeld;[26] extrapolation of their data to the typical embrittlement temperature (673 K) gives the diffusivity of 4.5×10^{-11} cm^2/s. According to these estimates, the Na diffusion in Al bulk is fast, and the diffusion of Na from bulk to GB should be even faster due to a very large driving force. Therefore, both thermodynamic and kinetic analyses indicate that Na can diffuse to the Al GB from bulk and will segregate on it.

The calculated interlayer distances for the GBs with Na in sites 1–3 and 6 are shown in Figs. 2(b)–2(e). There is a long-range oscillatory pattern for the Al interplanar distances away from the GB plane. When Na is in site 6, the distances between the sixth and the fifth and seventh layers are larger. The distance between the first layer and second layer ($d_{1\leftrightarrow2}$) is very large when Na is in site 2. For Na in site 3, the largest layer distance is between layer 3 and layer 4 ($d_{3\leftrightarrow4}$). All these cases are consistent with the larger Na atom expanding the layer distance.

For the GB with Na in sites 1–3 and 6, the calculated x displacements of each atom are plotted in Fig. 3(b)–3(e),

where it is found that some displacements are very large and cannot be ignored, especially when Na is in sites 2 and 3. There is also a long-range oscillatory pattern for the x displacements of each atom away from the GB plane. As discussed later, segregation of Na in site 3 causes reconstruction of the GB core, resulting in some x displacements as large as 0.905 a.u. This confirms that the full relaxation of the atom positions is necessary to obtain the lowest global total energy of the system.

All the calculated equilibrium expansion distances and segregation energies for each case are collected in Table II. We can see the GB expands significantly, by 0.95 a.u., when a Na atom segregates to site 1 compared with 0.45 a.u. expansion of the pure Al GB structure (taking the ideal CSL structure as reference). For this case, the segregation energy of Na is −0.84 eV/atom and the GB fracture energy is reduced to 0.987 J/m^2. The fracture modes will be described later.

B. Charge density

The charge density plays a key role in an analysis of interatomic bonding; the formation, dissolution, strengthening, and weakening of chemical bonds are always characterized by charge accumulation and depletion. Figure 5 shows contour plots of the calculated charge-density distribution for valence electrons in the (100) plane for the pure Al GB, and the Al GB with a substitutional Na atom in sites 1–3. Figure 5(a) shows that the Al atoms in site 2 and site −2 form a strong bond after structure relaxation. Comparing Figs. 5(a) and 5(b), inserting a Na atom in the core site reduces the charge density significantly in the area around the Na atom and the GB region and the range of the lower charge-density region caused by Na substitution extends along the z axis. The decreased charge density can be attributed to the small number of Na valence electrons, electron transfer from Na, and the expansion of the structure by the large Na atomic size.

In Fig. 5(c), replacing the Al atom in site 2 with a Na atom makes the charge density decrease more dramatically. The strong Al(2)-Al(−2) bond is replaced by a weak Al(2)-Na(−2) bond. Since site −2 is the most compressed atom site in the system, Na segregation into this site causes
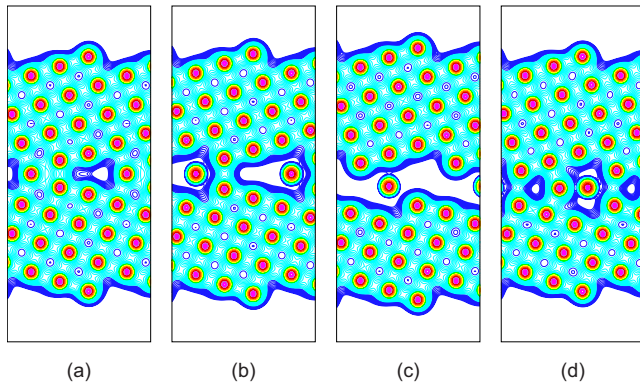
FIG. 5. (Color online) Calculated charge density for (a) pure Al GB, (b) Al GB with a Na atom in site 1, (c) Al GB with a Na atom in site 2, and (d) Al GB with a Na atom in site 3. Contours start from 0.01 $e/(\text{a.u.})^3$ and increase successively by a factor of $2^{1/8}$.

the GB to expand the most, by 2.00 a.u. This results in significantly reducing the strength of all bonding between the two grains. The Al(1)-Al(4) bond is already broken and the GB is essentially held together only by weak Na-Al bonds; it is therefore expected that the strength of this GB would be very low, as will be shown later.

In Fig. 5(d), the Na atom segregating into site 3 causes the GB structure and charge-density distribution to change dramatically. The Na atom in site 3 breaks the mirror symmetry of the GB but the relaxation and atomic rearrangements around the GB occur in a way that restores the mirror symmetry with a different mirror plane. Due to very weak Na-Al bonds, the Na atom in site 3 is able to detach itself and move into the large interstitial hole of the GB. This causes rearrangement of other GB atoms, and a new mirror plane is created, which contains Al(2) and Na(3) atoms. These atomic rearrangements allow the relaxed GB to accommodate a large Na atom without significant expansion of the GB—the expansion distance is only 0.50 a.u. in this case. The mirror plane of the system, which previously crossed site 1, now shifts down one layer. Although there is still a large charge density decrease in the area around the Na atom, it is less than in the cases of Na atoms segregating in sites 1 and 2 because now the Na atom effectively occupies the GB interstitial site. We can expect that the strength of this GB should be higher than the strength of GBs with a Na in sites 1 and 2—as will be demonstrated later. The effect of Na in site 3 is

complicated; it creates several possible fracture modes, as will be discussed in more detail below. In summary, the Na segregation in the Al GB induces GB expansion and a significant valence charge density decrease around the Na atom and along the GB plane, resulting in the formation of a weak bonding region.

C. Bond lengths

The bond length is very important for an analysis of interatomic bonding mechanisms. Figure 6 shows the calculated bond length around the GB plane schematically for the pure Al GB and the Al GB with a Na in sites 1–3.

Figure 6(a) shows the length of the bonds near the GB plane for the pure Al GB. There is mirror symmetry in the system. The shortest bond is the Al(2)-Al(−2) bond (4.847 a.u.) which is the strongest Al-Al bond in the pure Al GB system. Breaking the pure Al GB entails breaking the Al(1)-Al(2) bond, the Al(2)-Al(−2) bond, and the Al(1)-Al(4) bond. From the sort order of bond lengths $d^{2\leftrightarrow-2} < d^{1\leftrightarrow2} < d^{1\leftrightarrow4}$, the sort order of the strength of bonds is expected to be $E^{1\leftrightarrow4} < E^{1\leftrightarrow2} < E^{2\leftrightarrow-2}$. Therefore, we can expect that the Al(1)-Al(4) bond should break at first and the Al(2)-Al(−2) bond should break last when the GB fractures. This will be confirmed in the *ab initio* tensile test later.

Figure 6(b) shows the length of the bonds near the GB plane for the Al GB with a Na atom in site 1; there is still mirror symmetry in the system. Comparing Fig. 6(b) with Fig. 6(a), the large Na atom inserted in site 1 expands the GB and almost all the bond lengths increase. The strength of the Al(1)-Al(4) bond is weakened due to the increased bond length. The bonds between site 1 and site 4 and between site 1 and site −2 are Na-Al bonds whose lengths are much greater than the corresponding bonds in the pure Al GB system. From the bond length sort order, $d^{1\leftrightarrow4} < d^{1\leftrightarrow-2}$, the sort order of the strength of bonds is expected to be $E^{1\leftrightarrow4} < E^{1\leftrightarrow-2}$.

Figure 6(c) shows the length of the bonds near the GB plane for the Al GB with a Na atom in site 2. There is no mirror symmetry in the system. Comparing Fig. 6(c) with Fig. 6(a), the large Na atom inserted in site 2 expands the GB and almost all the bond lengths increase. The bond between site 2 and site −2 is a Na-Al bond in this case and its length is greater than that of the corresponding bonds in Figs. 6(a) and 6(b). The long Na-Al bonds between site 1 and site 2 and
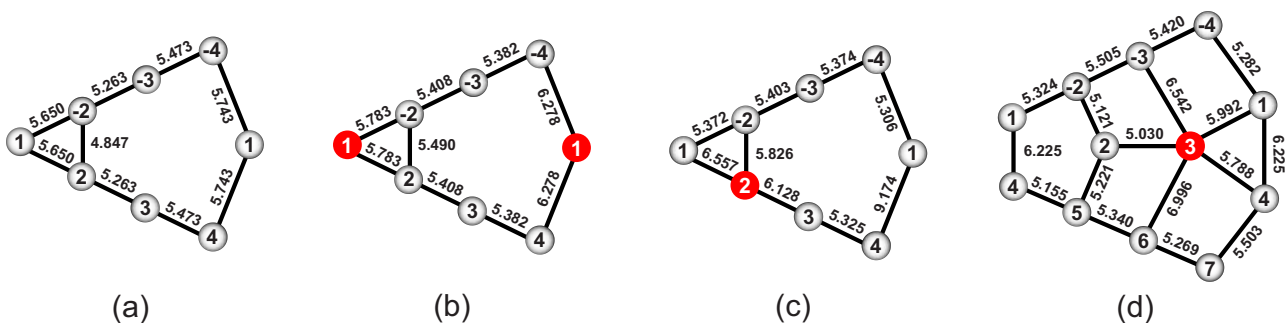
FIG. 6. (Color online) Schematics of calculated bond lengths (a.u.) for (a) pure Al GB, (b) Al GB with a Na atom in site 1, (c) Al GB with a Na atom in site 2, and (d) Al GB with a Na atom in site 3.

between site 2 and site 3 as well as the long Al-Al bond between site 1 and site 4 promote the formation of the weak charge-density region in Fig. 5(c).

Figure 6(d) shows the length of the bonds near the GB plane for the Al GB with a Na atom in site 3. Because the Na atom in site 3 relaxed into the GB interstitial site and the GB structure distorts significantly in this case, the GB mirror plane moves to the plane with site 2 and site 3. The mirror symmetry is rebuilt after relaxation in the system. Because the size of the two grains is not the same (12 and 14 layers, respectively) after the mirror plane moves down one layer, the mirror symmetry is not ideal. For example, the bond length of the bond between site 2 and site −2 slightly differs from the bond length between site 2 and site 5. It is expected that the ideal mirror symmetry would be obtained if a larger system is used to calculate. The Na-Al bonds between site 3 and site 2 are rather short compared with other Na-Al bonds in Fig. 6 because of the limited size of the GB vacancy. The Al-Al bond between site 1 and site 4 is similar to the bond between site 2 and site −2 in Figs. 6(a) and 6(b). However, its bond length is much longer than the latter.

D. Density of states

To further analyze the bonding characteristics of the Na-doped Al GB, we calculated the electronic densities of states (DOSs), which are presented in Fig. 7 for several atoms in the different systems. Figure 7(a) shows the local DOS (LDOS) for the central atom in a reference system of bulk Al calculated as a 25-layer slab, projected into the *s*- and *p*-electron contributions. It exhibits elements of fine structure in the form of small spurious peaks, which originate from the surface states of Al atoms at the slab boundaries. The overall shape, however, is similar to the DOS of bulk Al.

Figure 7(b), (1) and (2) shows the *s*- and *p*-electron contributions to the LDOS for atoms in sites 1 and 2, respectively, in the pure Al GB. There are notable differences from the bulk Al LDOS and the LDOS of the Al atom in site 1: pronounced packets of *s*-electron density separated by pseudogaps appear at −7.5, −6, −4, −2.5, and −1 eV [these are marked with arrows in Fig. 7(b), (1)], the pseudogap between bonding and antibonding *p* states is much less pronounced, and the centers of gravity of the occupied bands are shifted toward higher energy. These changes are the result of dissimilar local environments (cf. Fig. 1): the atom in site 1 of the GB has 12 first-nearest-neighbor Al atoms, as in bulk Al; however, all bond lengths and angles are different from those in bulk Al. The LDOS for the Al atom in site 2 is much more similar to that of the bulk Al; this atom has ten nearest-neighbor atoms, of which eight retain their local configuration (bond lengths and angles) close to that in bulk Al. Thus, the geometry of the local environment has a larger influence on the LDOS than the number of nearest neighbors.

Figure 7(c), (1) shows the LDOS for the Na atom replacing Al in site 1. The Na atom has one valence electron (vs the three of Al) but the electronic density on the Na atom in the GB is very low—much lower than 1/3 of Al—indicating that most of the Na electronic charge was transferred to Al atoms in the GB. This results in Na-Al bonding having a predomi-nantly ionic character. The remaining Na electrons partici-pate in the weak covalent bonding, as judged by the observed hybridization. These electrons are responsible for the forma-tion of small electronic "necks" between Na and Al which can be seen on the charge-density plots (Fig. 5). The metallic bonding which is characteristic for bulk Al is not observed for the Na atom.

The weak ionic bonding is expected to make the Na atom mobile and easily detachable from the GB surface after it separates. This may explain why Na is not detected on the fracture surface by experimental techniques. As we will show later, the ionic character of Na-Al bonding may also explain the peculiar behavior of the Na atom during GB separation (see Fig. 15): between 2 and 5 a.u. of separation the Na atom "hovers" between two Al grains without being attached to either.

Our results are in contradiction with the conclusions of Lu *et al.*,[6] who suggested that Na-Al bonds in the Σ9 Al GB have mostly metallic character. From our data, we can see that the electrons transferred from Na to Al do not participate in metallic bonding at the GB, as evidenced by the lack of electronic charge around Na atoms on the charge-density plots. Because Na has fewer electrons than Al, the electrons would have to transfer to Na from Al to sustain metallic bonding, which is the opposite of what we observe here.

The presence of Na on Al site 1 also leads to significant changes in the DOS of the Al atom on site 2 [see Fig. 7(c), (2)], especially for the *s*-electron states. The *s* electronic den-sity is pushed to higher energies and becomes more local-ized, forming two pronounced peaks at −7 and −5 eV. This is a manifestation of disruption and weakening of the bond-ing existing in the pure GB. These changes will result in an increase in the band contribution to the total energy, indicat-ing that the stability of the Al GB is reduced in the presence of segregated Na.

Thus, from a consideration of the electronic DOS we can conclude that segregated Na significantly weakens the Al GB by disrupting strong metallic Al-Al bonding and replacing it with very weak Na-Al bonding of mostly ionic character, which cannot resist decohesion. The small covalent Na-Al bonding contribution is insufficient to hold the Al GB to-gether under stress. Segregated Na also disrupts Al-Al bonds between grains that originate from bonding between Al at-oms in sites 2 and −2; the Na atom does so by both expand-ing the GB and modifying the electronic structure of Al atom in these sites.

VI. FRACTURE MODES AND ENERGY OF THE GB WITH SODIUM

The GB fracture modes and energies needed to cause the fracture can allow us to determine the way the GB fractures. The weakest bond path and fracture path are determined via first-principles calculations as well as a charge-density analy-sis. The fracture energy is defined as

$$\Delta E(fracture) = \frac{E_{FS1} + E_{FS2} - E_{GB}^{25\text{-}layer}}{S}, \qquad (7)$$

where $E_{GB}^{25\text{-}layer}$ is the total energy of a 25-layer Al GB with a Na atom, E_{FS1} and E_{FS2} are the total energies of the two Al

(a) Pure Al Bulk

(b) Pure Al GB

(c) Al GB + Na (site 1)
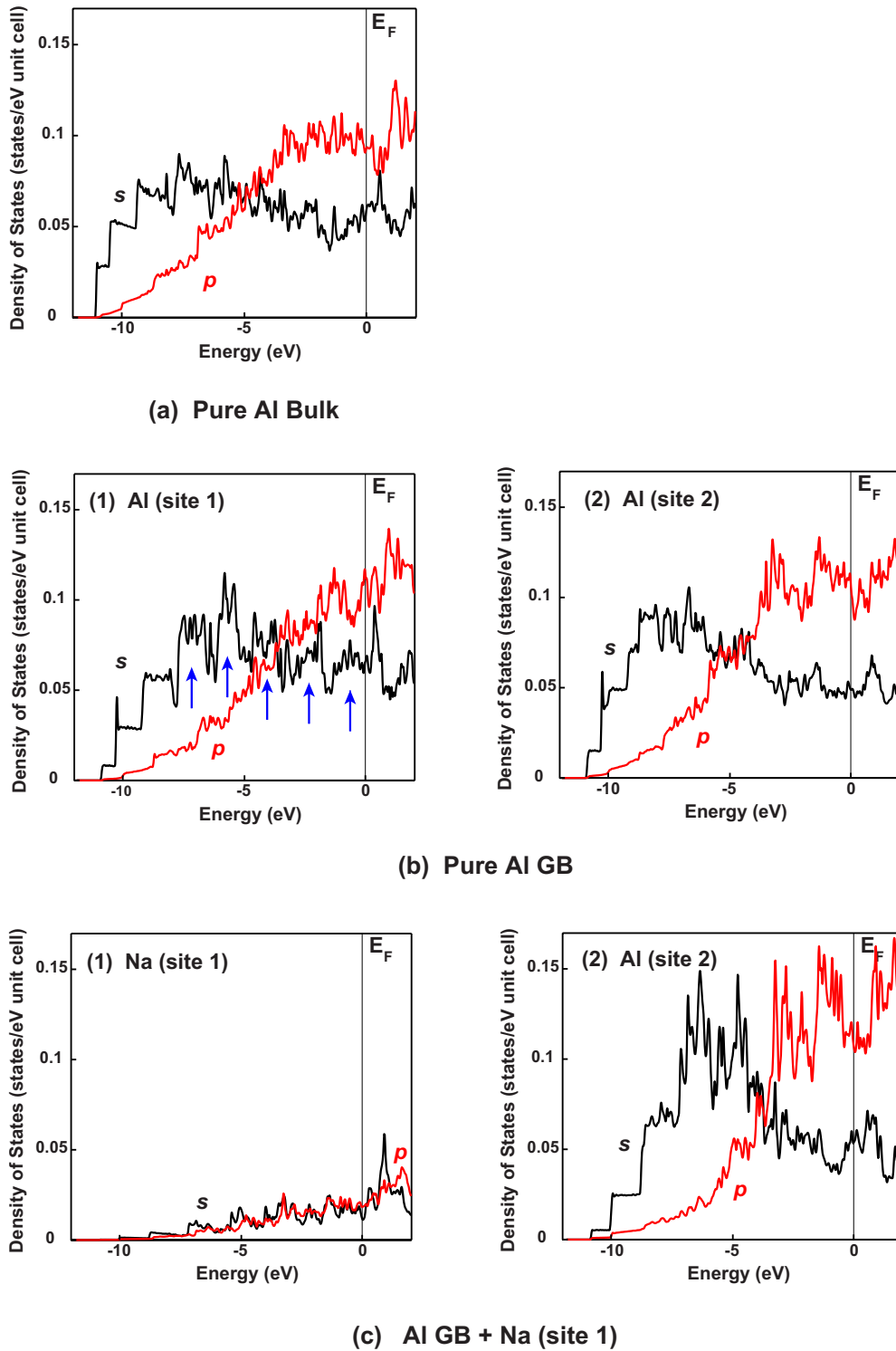
FIG. 7. (Color online) Calculated density of states with respect to the energy for (a) pure Al bulk; (b) pure Al GB, and (c) Al GB with Na in site 1. The Fermi energy is indicated by E_F.

(012) FSs obtained after GB breaking, and S is the unit cell area of the FS plane (012).

From the crystal structure in Fig. 1, it is easy to see that the bonds along the GB mainly include the bonds between atoms 1 and 2, 1 and −2, 2 and −2, 1 and 4, as well as 1 and −4. From the mirror symmetry in the pure Al GB, there is

only one possible GB fracture path for which the fracture energy is already calculated in Sec. IV.

If a Na atom segregates into the GB's site 1, the mirror symmetry of the GB remains. Similarly to the clean Al GB, only one fracture path is possible. After the GB breaks, one part is a 12-layer pure Al FS and the other is the 13-layer FS
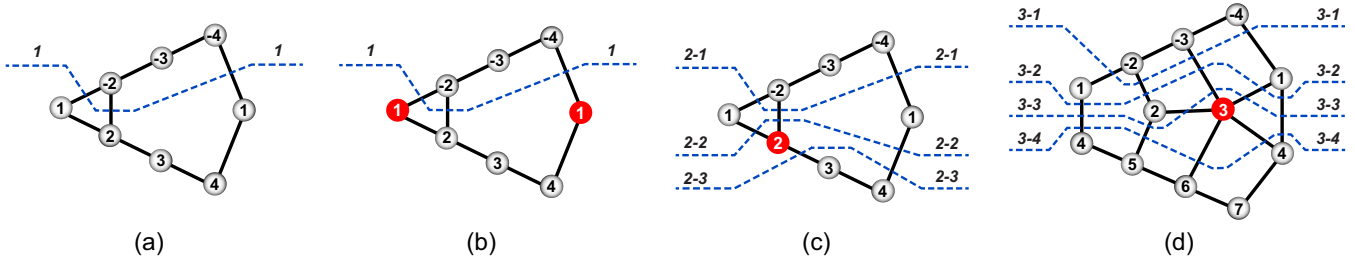
FIG. 8. (Color online) Schematics of all the fracture modes for (a) pure Al GB, (b) Al GB with a Na atom in site 1, (c) Al GB with a Na atom in site 2, and (d) Al GB with a Na atom in site 3. Fracture surfaces are marked with dashed lines.

with a Na atom. If a Na atom segregates into the asymmetrical sites 2 and 3, the mirror symmetry is broken, allowing two possible fracture modes according to the crystal structure in Fig. 1. In one mode, the core Al atom stays on the same grain with the Na atom; in the other mode, the core Al atom and the Na atom stay in different grains. After full relaxation, more fracture modes become possible according to the equilibrium atom sites and bonding analysis which will be discussed later.

The calculated charge density of the Al GB with a Na atom in site 2 is shown in Fig. 5(c). There is a weak charge-density region between the two grains because the large Na atom expands the system dramatically. The Na atom in site 2 forms a stronger bond with the upper grain than with the lower grain. The charge density in Fig. 5(c) shows that the strength of the Al(1)-Al(5) bond is much less than that of the Al(1)-Al(−5) bond and the bond length of the Al(1)-Al(5) bond is larger than that of the Al(1)-Al(−5) bond. Therefore, besides the two fracture modes which have been discussed above, there is another possibility in which the GB breaks into two parts. In this path, the bonds including the Al(1)-Al(5) bonds and the Na(2)-Al(3) and Na(2)-Al(6) bonds break while the Na(2)-Al(−2) bond remains. After the GB fractures in this path, two FSs form: one is the 14-layer FS with a Na and the other part is the 11-layer pure Al FS.

If a Na atom is in site 3 along the GB where the mirror symmetry is rebuilt after relaxation, from the calculated charge density shown in Fig. 5(d) and the length of bonds shown in Fig. 6(d), it is expected that the weak Al(1)-Al(4) bond might break for GB fracture; while the pair composed by the Al atoms in site 2 and Na atom in site 3, which form a short bond on the shifted "mirror plane," might stay with two different grains (upper or lower). Therefore, two more fracture modes are possible besides the two fractures modes which has been discussed above based on the ideal crystal structure in Fig. 1.

All the calculated fracture energies of possible modes with a Na in different sites are listed in Table II and the fracture modes are shown schematically in Fig. 8. If Na is in site 1 along the GB, the fracture energy is 0.987 J/m^2 which is much lower than the fracture energy of the pure Al GB (1.531 J/m^2). The large energy difference indicates that the strength of the GB decreases significantly when a Na atom replaces the Al atom in site 1.

If Na is in site 2, the fracture mode 2-1 shows that the fracture occurs along the GB plane with the core Al atom staying in the same grain (lower grain) containing the Na

atom. Its fracture energy is large (1.144 J/m^2). The fracture mode 2-2 is the way in which the fracture occurs along the GB plane with the core Al atom staying in the different grain (upper grain) without the Na atom. Its fracture energy is small (0.571 J/m^2). The fracture mode 2-3 has the lowest fracture energy of all modes in Table II. In this path, the Na atom stays in the 14-layer FS with the core Al atom. Compared with the calculated charge density in Fig. 5(c), it can be seen that the fracture mode with the lowest fracture energy follows the weak charge-density region along the GB.

If Na is in site 3, the fracture mode 3-1 has the highest fracture energy, which is even higher than the fracture energy of the pure Al GB. So this mode is not energetically favored. The fracture mode 3-2 in which the Na atom stays in the 12-layer FS without the core Al on site 1 has the lowest fracture energy compared with the other three modes in Table II. Checking with the equilibrium charge density in Fig. 5(d) and the bond length in Fig. 6(d), in this fracture mode the broken bonds include the bond between site 1 and site 4, the bond between site 2 and site −2, and the bond between site 3 and site 1. The fracture mode 3-3 has the fracture energy which is slightly larger than that of mode 3-2. In this mode, the broken bonds include the bond between site 1 and site 4, the bond between site 2 and site 5, and the bond between site 3 and site −3. The fracture mode 3-4 has a similar fracture energy to the fracture mode 3-2. Checking with the equilibrium charge density in Fig. 5(d) and the bond length in Fig. 6(d), the broken bonds include the bond between site 1 and site 4, the bond between site 2 and site 5, and the bond between site 3 and site 4 in this fracture mode. Owing to the mirror symmetry, the fracture mode 3-4 is equivalent to the mode 3-2 and their fracture energy should be the same. The small difference comes from the size effect of the two FSs after the GB fractures.

From Table II, it is evident that the Na has a different embrittling potency in the different fracture modes. This will be discussed later.

VII. EMBRITTLEMENT POTENCY OF Na WITH THE RICE-WANG THERMODYNAMIC MODEL

According to the Rice-Wang model, the total energy of five systems must be calculated with high precision in order to predict whether an impurity (M) is an embrittler or a cohesion enhancer to a hosting GB. These five systems are (1) the fully relaxed clean GB, (2) the fully relaxed GB with

impurity M, (4) the fully relaxed clean FS (3), the fully relaxed FS with M, and (5) a free M atom.

Quantitatively, the strength of the chemical interaction between an impurity and FS or GB is represented by its binding energy which, in the slab model, is defined as

$$\Delta E_{FS} = E(\text{Na/FS}) - [E(\text{FS}) + E(\text{Na})], \qquad (8)$$

$$\Delta E_{GB} = E(\text{Na/GB}) - [E(\text{GB}) + E(\text{Na})], \qquad (9)$$

where $E(\text{Na})$, $E(\text{FS})$, $E(\text{Na/FS})$, $E(\text{GB})$, and $E(\text{Na/GB})$ represent the total energies of the free Na atom, clean FS, Na adsorbed FS, clean GB, and Na segregated GB slabs, respectively. The embrittling potency is defined as

$$\begin{aligned} \Delta E &= \Delta E_{GB} - \Delta E_{FS} \\ &= [E(\text{Na/GB}) - E(\text{GB})] - [E(\text{Na/FS}) - E(\text{FS})]. \end{aligned}$$
$$(10)$$

All the calculated ΔE values are presented in Table II. For a Na atom in site 1, the calculated embrittling potency ΔE is +0.62 eV/atom. As the positive sign means an embrittling effect, Na in site 1 is an Al GB embrittler according to the Rice-Wang thermodynamic theory, and its embrittling potency is very strong.

For a Na atom segregated in site 2 of the GB, ΔE is +0.44 eV/atom in fracture mode 2-1, +1.10 eV/atom in fracture mode 2-2, and +1.19 eV/atom in fracture mode 2-3. All ΔE's are positive which indicates that Na is a strong embrittler in these modes. The fracture mode 2-3 has the lowest fracture energy and its embrittling potency is thus closest to reality. Therefore, ΔE is +1.19 eV/atom when Na is in site 2. Thus, the embrittling potency of Na segregated in site 2 is almost two times higher than for Na in site 1. This can be explained by the larger disruptive effect of Na in this position on bonding between GB grains, as evident from the calculated bonding charge densities shown in Fig. 5.

For a Na atom in site 3 of the GB, ΔE is +0.47 eV/atom in the facture mode 3-2 which has the lowest fracture energy. Na is an embrittler in this case. For the fracture mode 3-1, ΔE is −0.31 eV/atom and Na is a cohesion enhancer. However, this mode is so energetically unfavored that it cannot be practically realized. Since ΔE is +1.11 eV/atom in mode 3-3 and +0.48 eV/atom in mode 3-4, Na is an embrittler in both cases. Since the mode 3-2, with the lowest fracture energy, is favored, ΔE is +0.47 eV/atom and Na is an embrittler in site 3. This embrittling potency is smaller than for Na in sites 1 and 2, which again correlates with the observed characteristics of the bonding charge density shown in Fig. 5.

From these results, one can conclude that for the same impurity, its different position in the GB and the different fracture modes make it to be an embrittler or cohesion enhancer in the GB and its embrittling or strengthening effect can also be weak, moderate, or strong. Therefore, the position of the impurity in the GB and the different fracture mode has a significant effect on its embrittling or strengthening effect in the GB. Previous first-principles studies[10–14] did not consider these factors. The case with the most negative GB segregation energy and fracture energy (mode 1 in Table II) dominates over other cases energetically and is
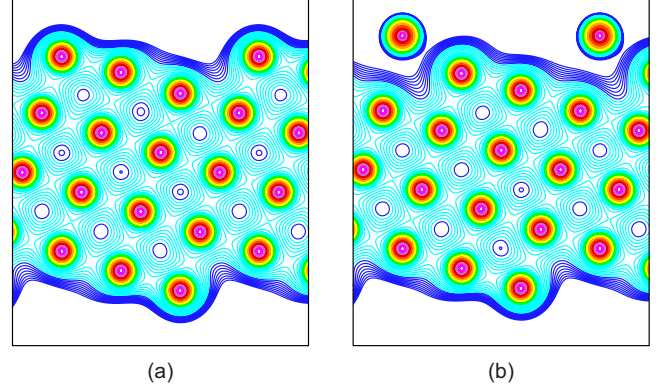
FIG. 9. (Color online) Calculated charge density for (a) pure Al 13-layer FS and (b) Al FS with a Na atom in site 1. Contours start from 0.01 $e/(\text{a.u.})^3$ and increase successively by a factor of $2^{1/8}$.

most close to reality. Therefore, when only one Na atom segregates into an Al GB, it will occupy site 1, where its embrittling potency is +0.62 eV/atom.

The calculated charge densities for the fractured surface of a pure Al GB and Al GB with a Na in site 1 is shown in Fig. 9, and the bond lengths near the surface of these cases are schematically represented in Fig. 10. Comparing the charge densities in Figs. 9(a) and 9(b) one can see that the strong metallic Al-Al bonding is replaced by weaker ionic Na-Al bonding. The Na-Al distances between site 1 and site 2 and between site 1 and site 4 are much longer than that of the corresponding Al-Al bond in Fig. 10(a). At the same time, the Al(2)-Al(3) and Al(2)-Al(5) bonds are shorter in the presence of Na in site 1, reflecting the fact that the Al(2) atom is now in the topmost layer, and a surface-layer compaction, traditionally observed in free-standing surfaces, takes place.

VIII. *AB INITIO* TENSILE TEST

The *ab initio* tensile test mimics the response of a GB to a uniaxial tensile strain normal to the GB plane. A series of complete *ab initio* tensile tests on the bulk Al (100) plane, clean Al GB and Al GB with a Na atom were performed. As schematically shown in Fig. 11, a uniaxial tensile strain is applied to the GB in its equilibrium configuration in the [012] direction which is normal to the GB plane (012). The fracture plane is assumed to be the GB plane at site 1. A unit cell is elongated in a series of increments up to 10.0 a.u., and in each case a separation, or a precrack, of a thickness that is equivalent to the unit cell elongation, is inserted between the
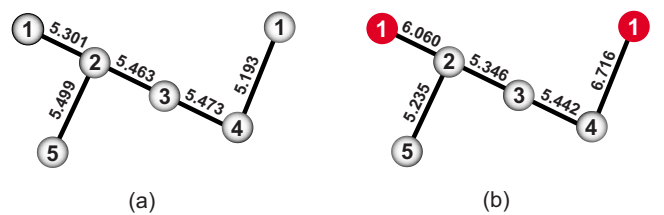
FIG. 10. (Color online) Schematic of calculated bond lengths (a.u.) for (a) pure Al 13-layer FS and (b) Al FS with a Na atom in site 1.
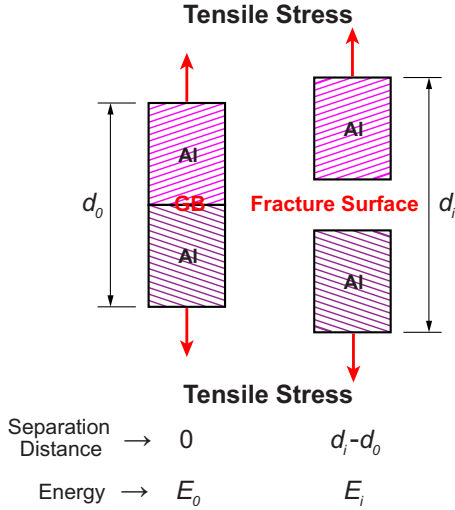
FIG. 11. (Color online) Schematic representation of the *ab initio* tensile test.

upper and lower crystal blocks at the fracture plane. For each separation distance, two kinds of calculations are performed: (i) rigid, i.e., without atomic relaxations, and (ii) with full atomic relaxations. For the relaxed z axis, three outermost layers on both blocks are fixed to keep the two crystal blocks separated and to simulate the bulklike environment inside grains. A series of total energies vs separation distance are thus obtained.

The separation energy ($2\gamma_i$), which is twice the surface energy γ_i, is obtained from the difference in the energy of the GB without separation and the energy with the specific separation distance i according to

$$2\gamma_i = \frac{E_i - E_0}{S},\tag{11}$$

where E_i is the total energy for the separation distance i, E_0 is the total energy of the equilibrium system without separation and S is the area of the GB (012) plane. The true separation energy, or the fracture energy, is defined as the limit of $2\gamma_i$ when $i \to \infty$ as

$$\Delta E(fracture) = 2\gamma = \lim_{i \to \infty} 2\gamma_i = \lim_{i \to \infty} \frac{E_i - E_0}{S}.\tag{12}$$

A universal binding energy relation (UBER) proposed by Rose *et al.*[27] was used to fit the separation energy of the rigid calculation,

$$f(z) = 2\gamma - 2\gamma(1 + z/\lambda)e^{(-z/\lambda)},\tag{13}$$

where 2γ is the fracture energy and λ is the characteristic separation length. Figure 12(a) shows the calculated rigid separation energies of Al bulk, the pure Al GB and the Al GB with Na in site 1 (solid squares) and their UBER fit. For a better direct comparison with the Al GB, the Al bulk is represented by a 25-layer slab model with (210) as a fracture plane—the same as the GB plane. Consistent with Eq. (13), the separation energy increases with separation distance very rapidly at the beginning, then increases more and more slowly until it reaches the true separation energy when the

separation distance is infinite. The rigid separation curves follow the UBER fit very well, and the limit of the separation energy at infinite separation distance can be calculated from this fit. At 10 a.u. separation, the separation energy almost reaches saturation, and its difference with the extrapolated limit is less than 1%. Since the separation energy indicates the energy needed to break the structure, it is a measure of the strength of the system and its resistance to crack initiation. Figure 12(a) attests that the strength of the pure Al GB is lower than that of Al bulk and that Na segregation in the Al GB weakens the GB greatly.

Figure 12(b) shows the relaxed separation energies of Al bulk, the pure Al GB and the Al GB with Na in site 1 (solid circles). Since relaxed separation curves do not follow the UBER, a fifth-degree polynomial was used to interpolate the data points. The separation curves have three distinctive regimes: at small separation distances, the precrack initially introduced in the model is "healed" and closed during relaxation, the two prefractured surfaces reconnect, and the resulting atomic configurations are equivalent to a uniform elongation of the system. In this elastic regime, the dependence of the separation energy on elongation closely follows Hooke's law and has a nearly parabolic character. At some critical elongation, however, the precrack cannot "heal" anymore. This situation is equivalent to an abrupt breakup of the system in an avalanche regime following the period of elastic elongation. (The avalanche breakup is marked by the dashed lines.) The avalanche breakup marks the point where atomic bonds between the two fracture surfaces actually break. At larger separations, the GB is already broken, and the separation energy increases slowly until saturation as the remaining long-ranged interaction forces between the two fractured surfaces vanish. The endpoints of this separation regime can be approximated with the UBER, and thus the limit of the separation energy at infinite separation can be extrapolated. Comparing rigid and relaxed separation curves [Figs. 12(a) and 12(b)], we can see that structural relaxation reduces the separation energy only slightly (by 0.07 J/m^2) for bulk Al and more significantly (by 0.20 J/m^2) for Al GB. This is the result of relaxing the internal stresses present in the GB. Comparing the separation energies between the three systems, we can see that the strength of Al bulk, 2.02 J/m^2, is reduced by 25%, to 1.52 J/m^2, in the presence of a GB. This approximately correlates with the number of Al-Al bonds per unit cell that are broken during separation. Segregated Na causes a dramatic reduction in the strength of Al GB, by 40%, to 0.90 J/m^2.

Another quantitative characteristic of the separation process is the "instability distance"—the expansion distance at which an avalanche breakup of the system occurs. It is dependent on the geometry of the computation cell; however, comparing the instability distances between systems of the same geometry allows one to make conclusions about the strength of the system and its resistance to breaking: the shorter the instability distance, the weaker is the system. The avalanche breaking of pure bulk Al occurs between 4.5 and 4.6 a.u. of separation while breaking of the pure Al GB— between 3.7 and 3.8 a.u. The Na-segregated GB does not exhibit a pronounced avalanche breakup, and its instability distance can be approximately estimated from the behavior
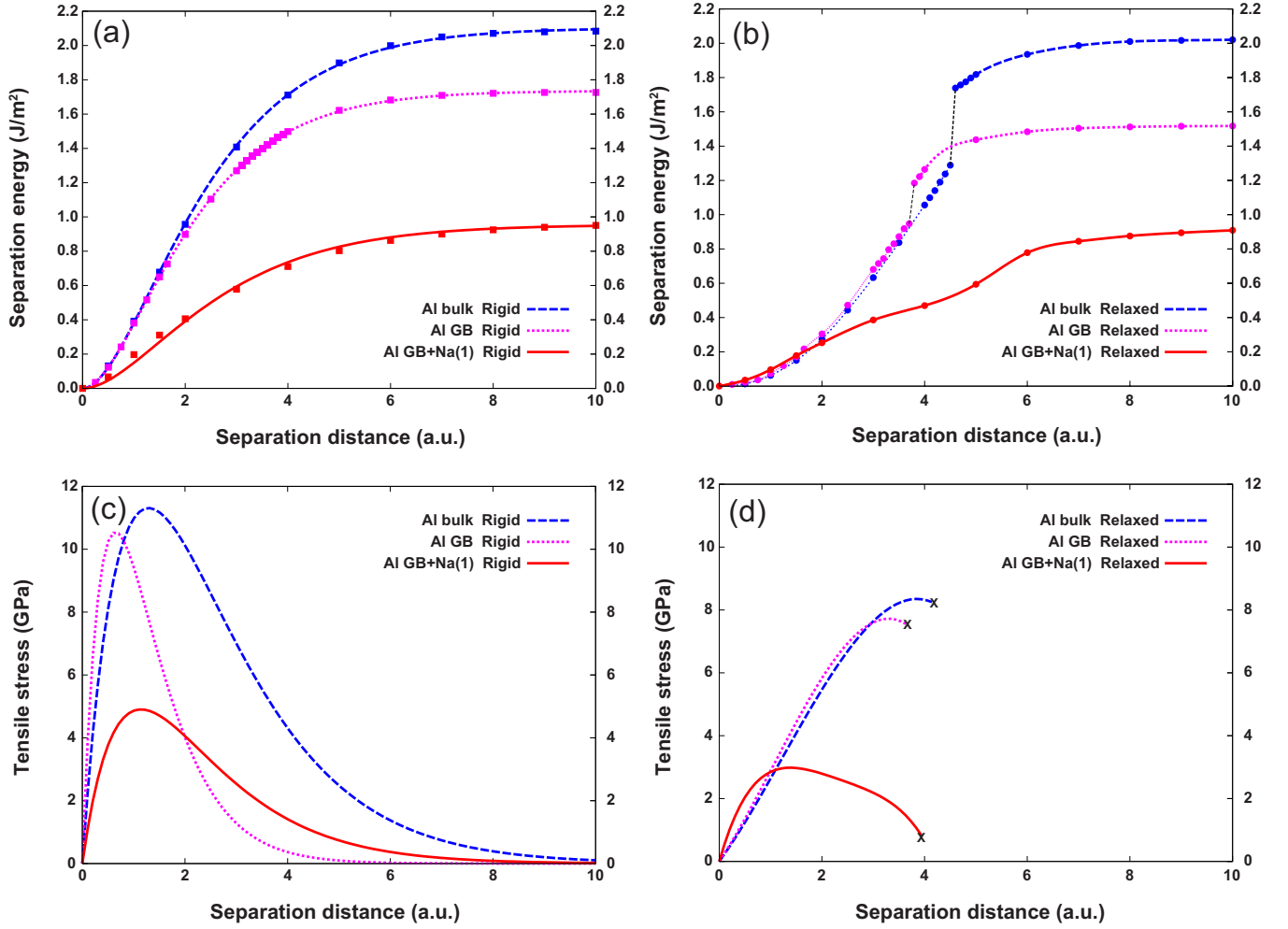
FIG. 12. (Color online) Calculated separation energies and tensile stresses vs separation distance of Al bulk, pure Al GB and Al GB with a Na atom in site 1 of from first principles. (a) Calculated separation energies from rigid calculations: solid squares are the calculated data points and the lines are their UBER fits. (b) Calculated separation energies from relaxed calculations: solid circles are the calculated data points and the lines are their polynomial fits. (c) Calculated tensile stresses from rigid calculations. (d) Calculated tensile stresses from relaxed calculations.

of the separation energy curve and charge densities (as shown below). It is considerably lower—between 2 and 3 a.u., thus again confirming a significant reduction in the GB strength by Na segregation.

From the separation energy curves the theoretical tensile stress σ can be calculated as $\sigma = \partial(2\gamma_i)/\partial(d_i - d_0)$, where $2\gamma_i$ is the separation energy as a function of separation distance $d_i - d_0$. For the rigid separation, which follows the UBER, the tensile stress can be calculated analytically and is plotted in Fig. 12(c) for Al bulk, the pure Al GB and the Al GB with Na in site 1. The quantity of most interest is the theoretical tensile strength, σ_{max}, which is the peak value of the tensile stress, and for the UBER fit σ_{max} is equal to $2\gamma/e\lambda$. From Fig. 12(c) one can see that σ_{max} is largest for bulk Al, at 11.6 GPa and only slightly smaller for pure Al GB, but Na segregation in the Al GB lowers σ_{max} by 57%. Figure 12(d) shows the calculated tensile stress of Al bulk, the pure Al GB and the Al GB with segregated Na for relaxed calculations. Since fifth-degree polynomials provide very good fits to the relaxed separation data [cf. Fig. 12(b)], we used analytic derivatives of these fit functions to calculate and plot tensile

stresses in relaxed calculations. The structure relaxation reduces the calculated theoretical tensile strengths but the relative absolute values remain the same: σ_{max} is largest for bulk Al (8.4 GPa), it is slightly smaller for pure Al GB, but Na segregation in the Al GB reduces σ_{max} almost threefold.

We will now find a relation between the embrittling potency of an impurity obtained within the Rice-Wang theory, and the separation energies obtained in theoretical tensile stress calculations. According to Eqs. (10) and (11), the separation energy is the total-energy difference between separated and initial GB cells divided by the area of the separated interface. Taking into account that separation of a GB in the limit of infinite separation essentially results in the creation of two FS configurations, FS1 and FS2, and assuming one segregated atom per unit area S, we have

$$2\gamma^{GB}S = E_{i \to \infty}^{GB} - E_0^{GB} = [E(FS1) + E(FS2)] - E(GB),$$

(14)
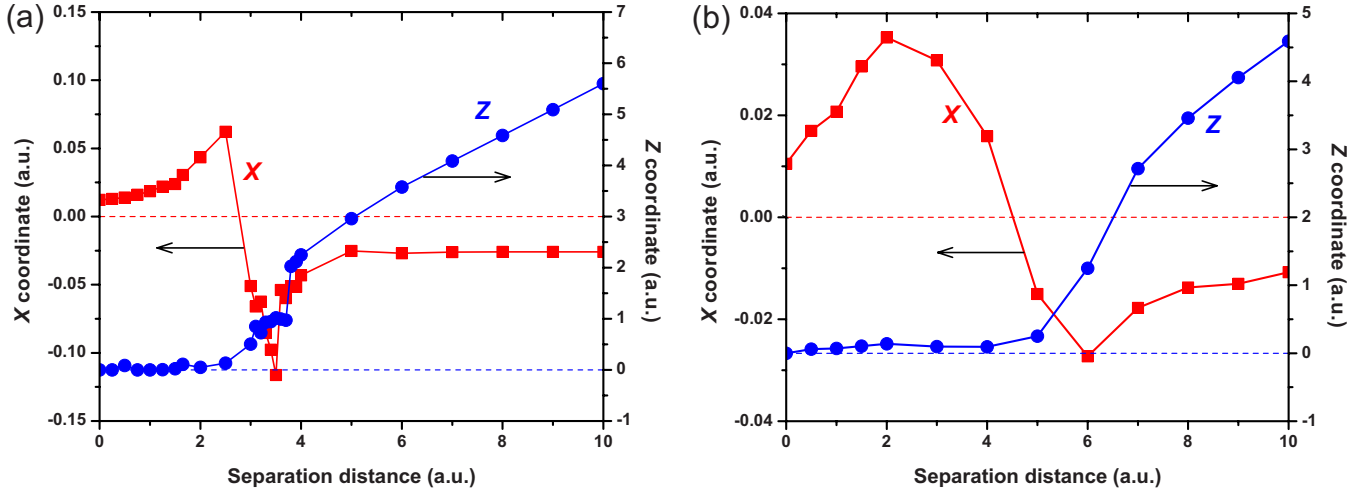
FIG. 13. (Color online) The variation in x and z coordinates of (a) the Al atom in the core of the pure Al GB and (b) the Na atom in the core of the pure Al GB with Na vs the separation distance during *ab initio* test.

$$2\gamma^{\mathrm{GB+Na}}S = E_{i\to\infty}^{\mathrm{GB+Na}} - E_0^{\mathrm{GB+Na}}$$

$$= [E(\mathrm{FS1}) + E(\mathrm{Na/FS2})] - E(\mathrm{Na/GB}). \quad (15)$$

Thus, the difference between the separation energies of pure Al GB and the Al GB with Na is

$$(2\gamma^{\mathrm{GB}} - 2\gamma^{\mathrm{GB+Na}})S$$

$$= [E(\mathrm{Na/GB}) - E(\mathrm{GB})] - [E(\mathrm{Na/FS1}) - E(\mathrm{FS1})]. \quad (16)$$

We can now see that Eq. (16) is equivalent to Eq. (10) which calculates is the embrittling potency of Na. The only difference is that $E(\mathrm{FS})$ in Eq. (10) is the total energy of the FS calculated in its own unit cell, and $E(\mathrm{FS1})$ in Eq. (16) is the total energy of the same FS calculated using the unit cell which contains two FS. These two values should be equal within the numerical accuracy of the calculations. Therefore, the embrittling potency can be determined from the *ab initio* tensile test calculations. Using Eq. (16), the calculated embrittling potency of Na is 0.61 eV/atom. This result agrees very well with the value obtained using the Rice-Wang model (0.62 eV/atom).

The variation in the x and z coordinates of the core Al in the pure Al GB system and the core Na in the Al GB with Na in site 1 during straining is shown in Fig. 13. In the pure Al GB [Fig. 13(a)] the x coordinate of the core Al atom increases slightly at initial steps of separation, then begins to move in the negative x direction after the separation distance reaches 2.5 a.u. At the 3.5 a.u. point, the x coordinate reaches its maximum negative value. From the 3.6 a.u. point on, the Al atom moves in the positive direction of the x axis. From the 5 a.u. point on, the x coordinate does not significantly change, which indicates that the broken grains are almost in equilibrium. The z coordinate increases very slowly at first implying that the Al-Al bond still exists; the z coordinate increases rapidly between 3.7 and 3.8 a.u. From the separation energy curve [Fig. 12(b)] we know that the GB breaks between 3.7 and 3.8 a.u. After the GB breaks, the z coordinate increases at the same pace as the separation distance.

Thus, an analysis of the variation in the x and z coordinates gives insights into the details of the GB separation. The separation between 0 and 2.5 a.u. follows an elastic regime, which is disrupted between 2.5 and 3.5 a.u. of separation. Correspondingly, the stress-strain curve [Fig. 12(d)] is almost linear. After 2.5 a.u., the separation starts to deviate from pure elastic behavior, which is evident from changes in both stress-strain behavior, and variation in the x and z coordinates of the core atom. The origins of this change will be discussed later. The second abrupt change in the x and z coordinates corresponds to the avalanche breakup of the GB.

The variations in the x and z coordinates of Na atom segregated in the Al GB in site 1 during straining, shown in Fig. 13(b), follow the same trend, but are less pronounced. The first change in behavior, which is limited to only the x coordinate, occurs between 2 and 3 a.u. of separation. The second change, involving both x and z coordinates, happens between 5 and 6 a.u. of separation, however, in contrast to the case of pure Al GB, is not abrupt, and the stress-strain curve does not show an avalanche breakup. To understand the origin of these differences, we will consider the bonding charge densities

Figure 14 shows the calculated charge density of the pure Al GB during straining with different separation distances. It can be seen that up to 3.7 a.u. of separation the GB is still intact. However, it can be also seen that the Al(1)-Al(4) bond breaks first, and at 3.0 a.u of separation it is already broken. It is not surprising, since we have determined previously from consideration of Al-Al bond lengths [Fig. 6(a)] that this bond is the weakest one. The breaking of this bond explains changes in the behavior of variations in the x and z coordinates in Fig. 13(a) and stress-strain behavior above 2.5 a.u. separation. The more dramatic changes occur between 3.7 and 3.8 a.u. of separation, when Al(1)-Al(2) and the Al(2)-Al(−2) bonds break simultaneously, causing abrupt changes in separation energy curve [Fig. 12(b) and x and z coordinates of the core atom (Fig. 13(a)]. Above 3.8 a.u. of separation, there are no noticeable changes in the charge density because the GB is already broken.

Figure 15 shows the calculated charge density of the Al GB with Na in site 1 during straining. As discussed earlier,

(a) *d*=0.0 a.u.   (b) *d*=3.0 a.u.   (c) *d*=3.7 a.u.   (d) *d*=3.8 a.u.   (e) *d*=4.0 a.u.   (f) *d*=10.0 a.u.
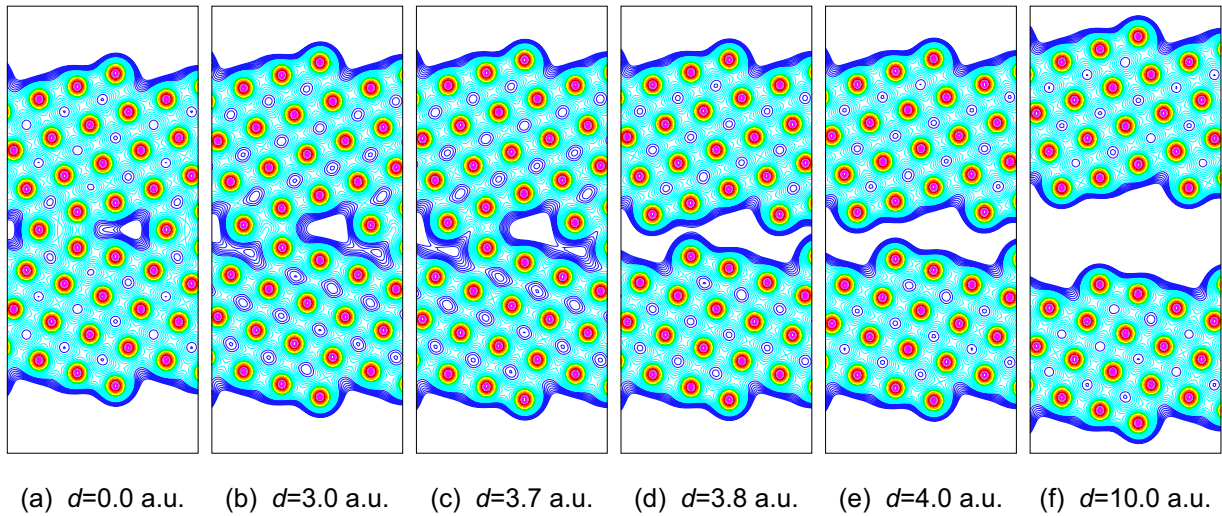
FIG. 14. (Color online) Calculated charge density of pure Al GB during *ab initio* tensile test with increasing separation distance *d*. Contours start from 0.01 $e/$(a.u.)^3 and increase successively by a factor of $2^{1/8}$.

Na changes bonding at the GB significantly by replacing strong Al-Al bonds with weak Na-Al bonds and weakening the Al(2)-Al(−2) bonds as a result of GB expansion due to the larger size of the Na atom. The Al(2)-Al(−2) bonds break at 2 a.u. separation (compared with 2.5 a.u. in pure Al GB), which is manifested in the changes in the behavior of the separation energy curve [Fig. 12(b)] and the *x* coordinate of the core atom [Fig. 13(b)]. The GB is now held together with Na-Al bonds. While weak, these ionic bonds are longer ranged, and hold the GB together up to 5 a.u. of separation. This results in a peculiar behavior of GB during breaking: the Na atom remains in the mirror plane, "suspended" between the two Al grains. The Na-Al bonds are also less rigid than the Al-Al bonds, and when the Na(1)-Al(2) bond finally breaks between 5 and 6 a.u., this does not lead to an avalanche breakup of the GB; however, there are notable changes in the behavior of the separation energy curve [Fig. 12(b)] and coordinates of this atom [Fig. 13(b)]. The Na

atom then moves off the mirror plane and attaches to the upper grain. Previously, from consideration of separation energy behavior and stress-strain curves (Fig. 12) it was established that the Na-segregated GB exhibits an instability between 2 and 3 a.u. of separation. It is now clear that this instability is only a first step of the two-step breakup process; it corresponds to breaking of the GB Al-Al bonds, which are significantly weakened by the presence of Na. In the second stage of separation the remaining Na-Al bonds break between 5 and 6 a.u., and the two grains become completely disjointed.

IX. COMPARISON WITH PREVIOUS EXPERIMENTAL AND THEORETICAL RESULTS

After performing multiple tensile test studies which showed that trace amounts of Na drastically reduce the ultimate tensile strength and reduction of area of the

(a) *d*=0 a.u.   (b) *d*=2 a.u.   (c) *d*=3 a.u.   (d) *d*=5 a.u.   (e) *d*=6 a.u.   (f) *d*=10 a.u.
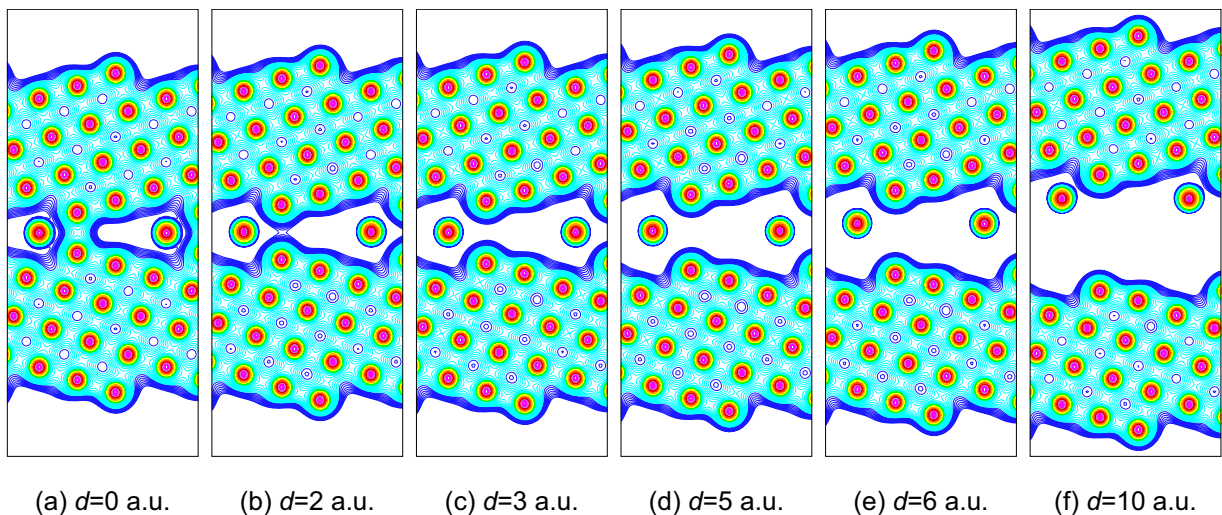
FIG. 15. (Color online) Calculated charge density of Al GB with a Na atom in site 1 during *ab initio* tensile test with increasing separation distance *d*. Contours start from 0.01 $e/$(a.u.)^3 and increase successively by a factor of $2^{1/8}$.

Al-5.5(mol %)Mg alloy, Horikawa *et al.*[4] attributed embrittlement primarily to segregation of Na atoms to GBs, although they were not able to detect sodium on intergranular fracture surfaces by AES. Using the calculated segregation energy and the McLean equation, we estimated that the segregated Na will almost saturate the Al GB at the equilibrium. Taken together with the experimental data on the diffusivity of Na in the Al bulk, this allowed us conclude that both thermodynamic and kinetic factors strongly favor Na segregation at the Al GB. Thus, our results confirm that the segregation of Na at the Al GB is the main cause of Na-induced embrittlement of Al as proposed by Horikawa *et al.*[4] Although the calculated tensile strength cannot directly compare with those from the experiment, our results agree qualitatively with the experimental observation that segregated Na causes a dramatic reduction in the strength of Al. The electronic density of states and charge-density analyses show that the Na-Al bonds are weak and have mostly ionic character which is expected to make the Na atom mobile and detachable from the fractured GB surfaces. This may provide an explanation of why Na is not detected on the fracture surface by AES. It was also argued that the detection limit of AES is not low enough, especially when the Na content is on the order of 1 ppm.[28] In fact, Na has been detected on the fracture surface successfully by secondary ion mass spectroscopy in Al-Li alloys when the Na content was hundreds of ppm in the bulk.[29]

Previous first-principles investigations by Lu *et al.*[6,7] showed that Na is an embrittler in the Al GB. Working with a different Al GB ($\Sigma 9(2\bar{2}1)[110]$ vs $\Sigma 5(012)[100]$ GB used in the present work), they obtained a smaller calculated segregation energy (-0.3 eV vs -0.84 eV in the present work), but a larger embrittling potency of Na ($+1.5$ eV/atom vs $+0.62$ eV/atom in the present work), and the theoretical tensile strength of the clean Al GB and the Na-doped Al GB also differs. Both the work by Lu *et al.*[7] and our work show that during the tensile test the Al-Al bond breaks first, followed by the Na-Al bond during strain for the Na-doped Al GB, in a two-step process. The similarity of the Na effect on two GBs with different geometries confirms that the embrittling effect of Na in Al is its intrinsic property related with features of its electronic structure and chemical bonding, and is not caused by specific GB structures. Our work provides a more comprehensive study and further clarification of the nature of Na-induced GBE with a detailed quantitative analysis, using the highly precise FLAPW method. We show

that the Na-Al bond in the Al GB is a weak ionic bond rather than the metallic bond suggested by Lu *et al.*[6] We further prove that the method using the Rice-Wang thermodynamic model and the method of *ab initio* tensile test are essentially equivalent, both of which confirm that Na is a strong intergranular embrittler.

X. CONCLUSIONS

A comprehensive *ab initio* investigation with the highly precise FLAPW method with GGA was carried out to reveal the mechanism of the Na-induced embrittlement of $\Sigma 5(012)[100]$ grain boundaries in Al at the electronic level. The pure Al GB and (012) Al FS were investigated, the equilibrium structures of GB and FS with sufficient sizes were determined, and the GB energy and FS energy were obtained. It was shown that Na exhibit a strong affinity to segregate at the Al GB with the segregation energy of 0.84 eV in its preferred position. The influence of sodium on the Al GB was investigated both within the framework of the Rice-Wang thermodynamic model and within the *ab initio* tensile test method. Through precise calculations, both methods confirm that Na is a strong intergranular embrittler with a potency of $+0.62$ eV/atom. An analysis of the results in terms of the relaxed atomic and electronic structures and their bonding characters shows that the aluminum-sodium bond has mostly ionic character and is very weak in both the GB and FS. The segregated Na causes embrittlement of the Al GB as a result of a combination of the following mechanisms: (i) size effect—the larger atomic size of Na segregating to the GB causes its expansion and weakens the strength of the Al-Al bonds across the two GB grains; (ii) electronic effect—by substitution of an Al atom by a Na atom, the stronger metallic Al-Al bonds are replaced by the much weaker Na-Al bonds. This work provides a fundamental quantitative understanding of sodium-induced GBE in Al alloys on the electronic level.

ACKNOWLEDGMENTS

*Corresponding author. FAX: +1-847-491-7820; shengjun-zhang@northwestern.edu

[1] S. F. Pugh, *An Introduction to the Grain Boundary Fracture in Metals* (The Institute of Metals, London, 1991).

[2] S. J. Zhang, Q. Y. Han, and Z. K. Liu, J. Alloys Compd. **419**, 91 (2006).

[3] G. D. Parkes, *Mellor's Modern Inorganic Chemistry* (Wiley, New York, 1967).

[4] K. Horikawa, S. Kuramoto, and M. Kanno, Acta Mater. **49**,

3981 (2001).

[5] S. Zhang, Q. Han, and Z. K. Liu, Philos. Mag. **87**, 147 (2007).

[6] G. H. Lu, A. Suzuki, A. Ito, M. Kohyama, and R. Yamamoto, Philos. Mag. Lett. **81**, 757 (2001).

[7] G. H. Lu, Y. Zhang, S. Deng, T. Wang, M. Kohyama, R. Yamamoto, F. Liu, K. Horikawa, and M. Kanno, Phys. Rev. B **73**, 224115 (2006).

[8] J. R. Rice and J. S. Wang, Mater. Sci. Eng., A **107**, 23 (1989).

[9] A. A. Griffith, Philos. Trans. R. Soc. London, Ser. A **221**, 163

(1921).

[10] R. Q. Wu, A. J. Freeman, and G. B. Olson, Science **265**, 376 (1994).

[11] R. Q. Wu, A. J. Freeman, and G. B. Olson, Phys. Rev. B **53**, 7504 (1996).

[12] L. P. Zhong, R. Q. Wu, A. J. Freeman, and G. B. Olson, Phys. Rev. B **55**, 11133 (1997).

[13] W. T. Geng, A. J. Freeman, R. Wu, C. B. Geller, and J. E. Raynolds, Phys. Rev. B **60**, 7149 (1999).

[14] W. T. Geng, A. J. Freeman, R. Wu, and G. B. Olson, Phys. Rev. B **62**, 6208 (2000).

[15] M. Yamaguchi, M. Shiga, and H. Kaburaki, Science **307**, 393 (2005).

[16] Y. Zhang, G. H. Lu, S. H. Deng, and T. M. Wang, Acta Phys. Sin. **55**, 2901 (2006).

[17] E. Wimmer, H. Krakauer, M. Weinert, and A. J. Freeman, Phys. Rev. B **24**, 864 (1981).

[18] G. C. Hasson and C. Goux, Scr. Metall. **5**, 889 (1971).

[19] M. L. Kronberg and F. H. Wilson, Trans. Am. Inst. Min., Metall. Pet. Eng. **185**, 501 (1949).

[20] J. P. Perdew, K. Burke, and M. Ernzerhof, Phys. Rev. Lett. **77**, 3865 (1996).

[21] W. Witt, Z. Naturforsch. A **22A**, 92 (1967).

[22] A. M. James and M. P. Lord, *Macmillan's Chemical and Physical Data* (Macmillan, London, UK, 1992).

[23] L. E. Murr, Acta Metall. **21**, 791 (1973).

[24] J. R. Smith and J. Ferrante, Phys. Rev. B **34**, 2238 (1986).

[25] D. McLean, *Grain Boundaries in Metals* (Oxford University Press, London, 1957).

[26] C. E. Ransley and H. Neufeld, J. Inst. Metals **78**, 25 (1950).

[27] J. H. Rose, J. Ferrante, and J. R. Smith, Phys. Rev. Lett. **47**, 675 (1981).

[28] H. Okada and M. Kanno, Scr. Mater. **37**, 781 (1997).

[29] D. Webster, Adv. Mater. Processes **145**, 18 (1994).